Franklin, Erick; Penteado, Marcos; Perissinotto, Rudolfo

The Motion of Grains of a Bed-Load Layer under a Turbulent Liquid Flow

ICHE 2014, Hamburg - Lehfeldt & Kopmann (eds) - © 2014 Bundesanstalt für Wasserbau ISBN 978-3-939230-32-8

The Motion of Grains of a Bed-Load Layer under a Turbulent Liquid Flow

E. Franklin, M. Penteado & R. Perissinotto
University of Campinas - UNICAMP, Campinas, Brazil

ABSTRACT: When a granular bed is sheared by moderate fluid flows, grains form a moving granular layer, known as bed load, which stays in contact with the fixed part of the bed. Although of importance for many scientific domains, the displacement of individual grains in the moving bed is not well understood. This paper presents an experimental investigation on the motion of grains of a granular bed sheared by a liquid flow. In our experiments, fully-developed turbulent water flows were imposed over a granular bed of known granulometry. The tested conditions were close to incipient bed load, and therefore the thickness of the bed-load layer was of the order of the grains diameter. Different tested conditions corresponded to different water flow rates. The water stream over the moving bed was measured by Particle Image Velocimetry and the displacements of grains were filmed with a high-speed camera. The trajectories of individual grains were determined by post-processing the images, and the typical lengths and velocities were computed afterwards. Finally, the motion of grains was correlated to the water flow conditions, and the bed-load transport rate was estimated and compared with semi-empirical transport rate equations.

Keywords: Sediment transport, Bed load, Water stream, Turbulent boundary layer

1 INTRODUCTION

Sediment transport by shear flows is frequently found in both nature and industry. When the shear forces are moderate with respect to the grains weight, grains settle and a granular bed is formed. In this case, a moving granular layer takes place in which the grains stay in contact with the fixed part of the granular bed. This kind of transport, known as bed load, is present in the displacement of riverbeds, in the transport of sand by wind, and in the transport of sand in petroleum pipelines. Although of importance for many scientific domains, the displacement of individual grains within the moving bed is not well understood. The knowledge of the typical trajectory of individual grains is necessary for the correct predictions of the bed-load transport rate and to fully understand the perturbation of the fluid flow by bed load (solely), known as "feedback effect" (Bagnold, 1941; Recking et al., 2008).

Bagnold (1941) studied the transport of sand in deserts and the dynamics of desert dunes. The author showed that in the aeolian case individual grains effectuate ballistic flights whose length scale is many times greater than the grain diameter. Given the large grain to fluid density ratio, bed load in air occurs under high Reynolds numbers that correspond to hydraulic rough regimes. Therefore, the moving granular layer takes place in the overlap sublayer of the turbulent boundary layer (unperturbed). In liquids, given the small grain to fluid density ratio (around unity), bed load takes place under moderate Reynolds numbers that correspond to hydraulic smooth or transitional regimes. In this case, the thickness of the moving granular layer is of a few grain diameters, and therefore bed load occurs in regions that correspond to the viscous or the buffer sublayers of turbulent boundary layers.

In the past decades, many studies were devoted to bed load, e.g., Bagnold (1941), Meyer-Peter and Müller (1948), Bagnold (1956), Lettau and Lettau (1978) and Charru et al. (2004). Charru et al. (2004) presented an experimental work on the dynamics of a granular bed sheared by a viscous Couette flow in laminar regime. The experimental results concerned the displacement of individual grains (velocities, du-

rations and lengths), and the surface density of the moving grains. For a given fluid shear stress (at a given flow rate) and an initially loosely packed bed, Charru et al. (2004) showed that the surface density of moving grains decay while their velocity remains unchanged. They proposed that this decay is owed to an increase in bed compactness (caused by the rearrangement of grains, known as armouring), causing then an increase in the threshold shear rate for bed load. They found that the velocity of individual grains is given by the shear rate times the grain diameter times a constant factor approximately equal to *0.1*, and that the duration of displacements is approximately *15* times the settling time (considered as the grain diameter divided by the settling velocity of a single grain). Charru et al. (2004) proposed that the mean displacement varies with the Shields number (presented next), and reported values between *1* and *5* times the grain diameter (within the range of Shields number of their experiments).

Concerning the bed-load transport rate, there is no definite expression (Gomez and Church, 1989; Nakato, 1990). From dimensional analysis, two dimensionless groups are necessary to determine the bed-load transport rate. Usually, the dimensionless groups are chosen as the Shields number θ and the particle Reynolds number Re_* (Raudkivi, 1976). The Shields number is the ratio of the entraining to the resisting forces and the particle Reynolds number is the Reynolds number of the fluid at the grain scale. They are given by Eqs. (1) and (2), respectively.

$$\theta = {\tau}/{(\rho_s - \rho)gd} \tag{1}$$

$$Re_* = {u_* d}/{\nu} \tag{2}$$

where τ is the shear stress caused by the fluid on the granular bed, d is the grain diameter, g is the gravitational acceleration, ν is the kinematic viscosity, ρ is the specific mass of the fluid and ρ_s is the specific mass of the grain. In the case of two-dimensional turbulent boundary layers, the shear stress is $\tau = \rho u_*^2$, where u_* is the shear velocity, and u is the mean velocity in the overlap region, given by:

$$u^+ = \frac{1}{\kappa} ln\left(\frac{y}{y_0}\right) \tag{3}$$

or

$$u^+ = \frac{1}{\kappa}\ln(y^+) + B \tag{4}$$

where $\kappa=0.41$ is the von Kármán constant, y_0 is the roughness length, $u^+=u/u_*$ is a dimensionless velocity, $y^+=yu_*/\nu$ is the vertical distance normalized by the viscous length, and B is a constant. Equations (3) and (4) are equivalent, Eq. (3) being generally employed for hydraulic rough regimes and Eq. (4) for hydraulic smooth regimes (for which $B=5.5$).

In the aeolian case, Bagnold (1941) showed that the presence of bed load changes the overlap layer of turbulent boundary layers. This is known as "feedback effect" and is caused by the momentum transfer from the air flow to the salting grains. Because the bed-load thickness in air is many times greater than the grain diameter, the feedback effect is relatively easy to be quantified in the aeolian case (e.g., Rasmunsen et al., 2006; Bauer, 2004; Yang et al. 2007). The feedback effect also occurs in liquids, however, given the small thickness of the moving layer and the small grain to fluid density ratio, it is lower than in the aeolian case and difficult to be quantified.

Recently, Franklin et al. (2014) presented an experimental work on the feedback effect in liquids. The authors measured the velocity profiles of turbulent liquid flows over moving granular beds in conditions close to the incipient motion of grains. The experiments were performed in a horizontal channel of rectangular cross-section, which is the same channel used in the present work (presented in next section). The turbulent velocity profiles were measured by Particle Image Velocimetry at the vertical symmetry plane of the channel, and the feedback effect was quantified. The experimental results showed a good agreement between the water profiles over moving beds and the law of the wall in the region close to the granular bed, indicating that the flow is in local equilibrium in this region. Also, although in the hydraulic smooth regime, the bed-load effect on the water stream is the vertical displacement of the normalized velocity profiles. This means that the feedback effect in smooth regime is equivalent to a roughness length increase in the rough regime. Franklin et al. (2014) reported values of shear velocity u_*, roughness length y_0, and constant B measured for moving beds of different granulometries.

2 EXPERIMENTAL DEVICE

The experimental device consisted of a water reservoir, a progressive pump, a flow straightener, a *5m* long transparent channel of rectangular cross section (*160mm* wide by *50mm* high), a settling tank and a return line. The flow straightener consisted of a divergent-convergent device filled with a porous media. The channel test section was *1m* long and started at *40* hydraulic diameters (*3m*) downstream of the channel inlet. At the channel's developing section a fixed granular bed was inserted, composed of glass spheres glued on the surface of PVC plates, whose thickness was *7mm*. In the test section, loose grains were deposed and formed a loose granular bed whose thickness was *7mm*. The fixed and granular beds were of same granulometry. This assured a *3m* entrance length of same granulometry and of same thickness as the loose bed. Downstream the test section, a *1m* long section connected the test section exit to a settling tank. A layout of the experimental device is presented in Fig. 1.

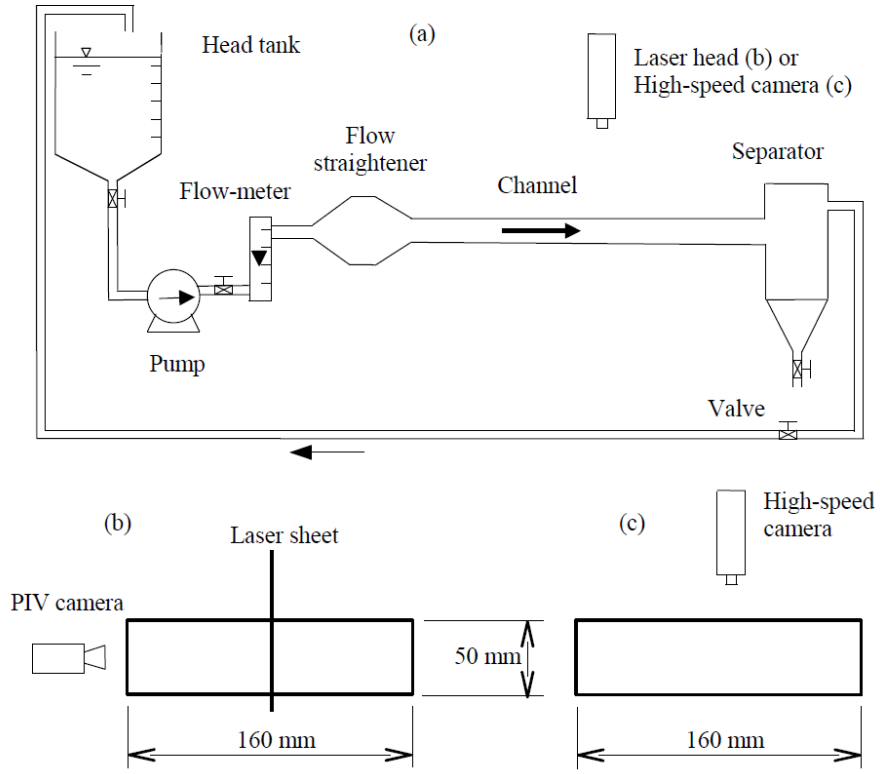

Figure 1. Scheme of the experimental loop: (a) side-view; (b) channel cross section (PIV tests); (c) channel cross section (tests with the high-speed camera).

For the high-speed movies, the employed grains consisted of glass spheres with specific mass of ρ_s=*2500 kg/m*^{3} and size ranging from d = *400 μm* to d = *600 μm*, and it is assumed that the mean diameter was d_{50}=*500 μm*. In order to facilitate the post-treatment of images, *5 %* of the granular bed consisted of black glass spheres (of same granulometry and material). Prior to the tests, the loose granular bed was smoothed and leveled, with the channel already filled up with water. Next, the water flow rates were established by adjusting the pump's frequency.

For the experiments with Particle Image Velocimetry, flow rates of approximately *5, 5.5, 6, 6.5, 7* and *7.5 m*^{3}*/h* were employed. They correspond to cross-section mean velocities in the range $0.19m/s \leq \bar{U} \leq 0.30m/s$ and to Reynolds number $Re = 2H_{gap}\bar{U}/\nu$ in the range *16000* < *Re* < *27000*, where H_{gap} is the distance from the granular bed to the top wall. These tests measured the water flows over the moving beds and are described in detail in Franklin et al. (2014). For the experiments with high-speed camera, the flow rates were of *4.8, 6.3, 6.5, 6.5* and *7.1 m*^{3}*/h*, corresponding to $0.19m/s \leq \bar{U} \leq 0.29m/s$ and *16000* < *Re* < *25000*. These tests measured the displacement of the grains on the bed surface.

2.1 *Water Stream*

Particle Image Velocimetry was employed to obtain the instantaneous velocity fields of the water stream, and the experiments are described in detail in Franklin et al. (2014). The light source was a dual cavity

Nd:YAG Q-Switched laser, capable to emit at *2 x 130mJ*, and its power was fixed to within *65%* and *75%* of the maximum power to assure a good balance between image contrasts and undesirable reflection from the granular bed. Suspension of particulate already present in tap water together with hollow glass spheres of *10 μm* and specific gravity *S.G .= 1.05* were employed as seeding particles. The PIV images were captured by a CCD (charge coupled device) camera acquiring pairs of frames at *4 Hz* with a spatial resolution of *2048 px x 2048 px*. The total field was around *75 mm x 75 mm*. The computations were made with interrogation areas of *8px x 8px* and *50 %* of overlap, which corresponds to *512 x 512* interrogation areas and *0.14 mm x 0.14 mm* of spatial resolution.

2.2 *Granular Flow*

A high-speed CCD camera was employed to obtain the displacements of grains. For our tests, the camera frequency was set between *80 Hz* and *400 Hz* with a spatial resolution of *1280 px x 1024 px*. The total field was between *832 mm²* and *3250 mm²* and a makro-planar lens of *50 mm* focal distance was used. For all the tests, the number of acquired images was *1415*.

The trajectories and velocities of individual grains were determined by post-processing the images with the *Motion Studio* software as well as with *MatLab*. For each test, the trajectories of grains were determined by identifying and following the black spheres in all the movie frames. The quasi-instantaneous velocities were then determined by multiplying the inter-frame displacements of individual grains by the camera frequency.

3 EXPERIMENTAL RESULTS

3.1 *Water Stream*

Franklin et al. (2014) measured water flow profiles over moving beds whose grains consisted of glass spheres with ρ_s=*2500 kg/m³* and classified in two populations. One of these populations had its size ranging from *d = 300 μm* to *d = 425 μm*, and it was assumed that d_{50}=*363 μm*. For granular beds of this granulometry, three series of tests were performed by increasing in steps the water flow rate (from the value corresponding to the bed-load threshold) and performing PIV measurements for each step. The shear velocity u_*, the particle Reynolds number Re_*, the Shields number θ, and the mean cross-section velocity $\overline{U}$ for each water flow rate Q are shown in Tab. 1.

Table 1. Water flow rate Q, mean cross-section velocity $\overline{U}$, shear velocity u_*, particle Reynolds number Re_*, and Shields number θ for the water stream over a moving granular bed (Franklin et al., 2014).

Q (m³/h)	$\overline{U}$ (m/s)	u_* (m/s)	Re_*	θ	Q (m³/h)	$\overline{U}$ (m/s)	u_* (m/s)	Re_*	θ
5.3	0.21	0.0130	5	0.03	6.7	0.27	0.0168	6	0.05
5.8	0.23	0.0136	5	0.03	7.7	0.29	0.0228	8	0.10
6.1	0.25	0.0145	5	0.04	5.4	0.21	0.0126	5	0.03
6.8	0.27	0.0171	6	0.05	5.9	0.23	0.0136	5	0.03
5.3	0.21	0.0133	5	0.03	6.4	0.26	0.0153	6	0.04
5.9	0.24	0.0149	5	0.04	6.8	0.27	0.0162	6	0.05
6.3	0.25	0.0145	5	0.04	…	…	…	…	…

3.2 *Granular Flow*

The moving granular bed was filmed with a high-speed camera and the trajectories of individual grains were then determined by post-processing the images.

Figure 2(a) presents the x and y position components of a given glass sphere as function of time t, and Fig. 2(b) presents the x and y velocity components of a given glass sphere as function of time t, both for Q = *6.8 m³/h*. In these figures, x and y are, respectively, the longitudinal and the transverse components of the position vector, and v_x and v_y are, respectively, the longitudinal and the transverse components of the velocity vector. The continuous and the dashed curves correspond to the x and y components, respectively.

Figure 2(a) shows that the displacement of individual grains is intermittent, with periods of acceleration, deceleration and at rest, which is corroborated by Fig. 2(b). For this water flow rate, the typical grain displacement is ≈$5d_{50}$.

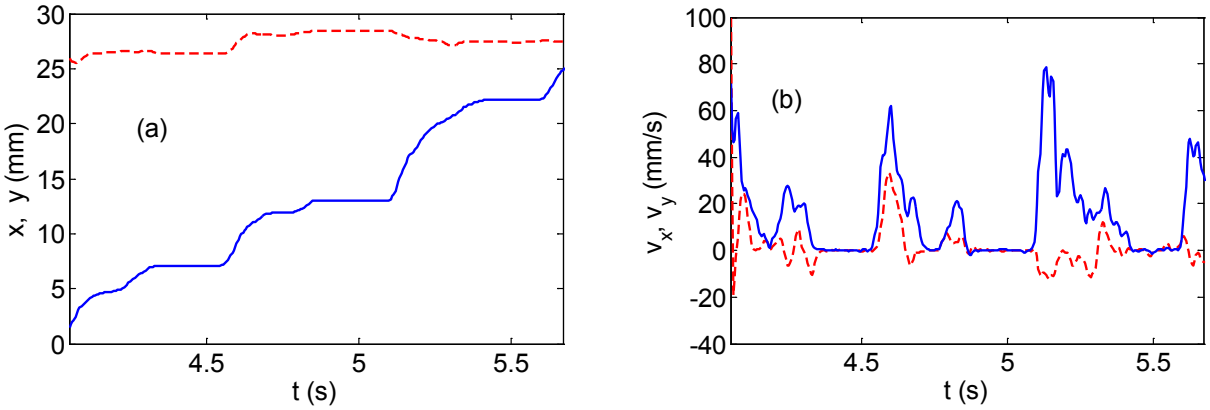

Figure 2. (a) Displacement of an individual grain. (b) Velocity of an individual grain. Q = 6.8 m^3/h.

The longitudinal displacement of each moving black sphere was computed as the distance traveled by the sphere between periods at rest, and the mean longitudinal displacement Δx was determined by averaging the longitudinal displacement of black spheres for each water flow rate. Therefore, Δx corresponds to the typical longitudinal distance traveled by grains between periods at rest for a given water flow condition. Table 2 shows Δx as well as the standard deviation of the longitudinal displacement of grains $\sigma_{\Delta}x$. The mean longitudinal displacement normalized by the grain diameter $\Delta x^{ad} = \Delta x/d_{50}$ is also shown in Tab. 2, and it is seen to vary between *8.2* and *22.6*.

Table 2. Water flow rates Q, mean longitudinal displacement of grains Δx, standard deviation of the longitudinal displacement $\sigma_{\Delta}x$, mean displacement velocity U_d, standard deviation of the longitudinal velocity σ_{Ud}, normalized longitudinal displacement Δx^{ad}, normalized displacement time t_d^{ad}, normalized mean displacement velocity U_d^{ad}, number of black spheres that crossed a transverse line during the total time of the movie N_L and movie frequency f.

Q (m^3/h)	Δx (mm)	σ_{Δ}x (mm)	U_d (mm/s)	σ_{Ud} (mm/s)	Δx^{ad}	t_d^{ad}	U_d^{ad}	N_L	f Hz
4.8	4.1	2.0	21.1	2.7	8.2	28.7	0.33	18	50
5.7	5.6	3.8	44.9	14.3	11.2	18.3	0.48	5	200
6.3	9.4	3.7	39.0	8.0	16.8	35.0	0.35	124	90
6.5	9.9	4.3	40.9	7.4	19.8	35.4	0.33	78	90
6.5	5.8	2.3	36.0	8.0	11.6	23.7	0.29	27	200
6.8	6.9	1.7	45.0	13.9	13.8	22.5	0.30	30	200
7.0	7.4	4.8	66.0	15.1	14.8	16.5	0.39	47	120
7.1	11.3	5.7	45.3	11.2	22.6	36.9	0.25	250	150
7.5	8.8	5.3	58.0	19.1	17.6	22.3	0.28	30	400
8.1	6.5	3.6	59.5	16.4	13.0	15.9	0.25	74	300

The longitudinal velocity of moving grains was computed by considering only the periods for which each black sphere was moving, i.e., the periods of acceleration and deceleration. The mean displacement velocity U_d was then obtained by averaging all the longitudinal velocities, for each water flow rate. It is presented in Tab. 2 together with the standard deviation of the longitudinal velocity, σ_{Ud}.

The mean displacement velocity was normalized by the shear rate and the grain diameter $U_d^{ad} = \nu U_d(u_*^2 d_{50})^{-1}$ and is shown in Tab. 2. In all tested conditions, $U_d^{ad} = ord(0.1)$ (where *ord* denotes order of magnitude), in agreement with Charru et al. (2004). The mean displacement time was computed as $t_d = \Delta x/U_d$, and it corresponds to the time taken by individual grains to travel the typical displacement distance Δx at the typical displacement velocity U_d. The mean displacement time was normalized by the grain diameter and the settling velocity $t_d^{ad} = t_d U_s/d_{50}$, where U_s is the settling velocity of a single grain. The normalized displacement time is shown in Tab. 2. The settling velocity was computed by the Schiller--Naumann correlation (Clift et al., 2005). The computed values of t_d^{ad} are between *15.9* and *36.9*, in agreement with Charru et al. (2004).

Based on the number of black spheres that crossed a given transverse line during the total time of the movie N_L and on the camera acquisition frequency f, both shown in Tab. 2, the volumetric bed-load transport rate was estimated as $Q_B = (160/L_{image})(f/1415)(N_L/0.05)\pi d_{50}^3/6$ and was normalized by the refer-

ence flow rate (Raudkivi, 1976) as $\phi_B = (Q_B /0.16)((S-1)g\, d_{50}^3)^{-0.5}$, where $S = \rho_s/\rho$. Both Q_B and ϕ_B are shown in Tab. 3.

The bed-load transport rate estimated from the displacement of individual grains (presented in Tab. 3) is next compared with semi-empirical expressions. One of the most employed expressions is that of Meyer-Peter and Müller (1948), based on data from exhaustive experimental work, and for this reason it is used here. This expression is given by $\phi_B = a(\theta - \theta_{th})^{3/2}$, where θ_{th} is the Shields number corresponding to the threshold shear stress, $a=8$ if both form drag (due to ripples) and skin friction are considered, and $a=4$ if only the skin friction is considered (Wong and Parker, 2006). Ripples were absent in our tests, therefore $a=4$ in the following. As shown by Charru et al. (2004), the threshold shear stress may grow during time because of an increase in bed compactness. They proposed that the increase in bed compactness is caused by the grains movement, so that, when close to incipient motion, it occurs faster under higher shear stresses. Given the sequence in which the present tests were performed, the values of θ_{th} are expected to vary with the water flow rate. For this reason, the values of θ_{th} were varied between 0.015 and 0.045, which are values expected for loose beds. The corresponding values, varied in order to follow roughly the Meyer-Peter and Müller (1948) expression, are presented in Tab. 3.

Table 3. Water flow rates Q, bed-load transport rate Q_B, Reynolds number Re, shear velocity u_* , particle Reynolds number Re_*, Shields number θ, non-dimensional bed-load transport rate ϕ_B and estimated threshold Shields number θ_{th}.

Q (m3/h)	Q_B (m3/s)	Re	u* (m/s)	Re*	θ	ϕ_B	θ_{th}
4.8	0.02×10^{-7}	1.7×10^4	0.0112	6	0.017	0.0003	0.015
5.7	0.03×10^{-7}	2.0×10^4	0.0137	7	0.026	0.0004	0.020
6.3	0.25×10^{-7}	2.2×10^4	0.0149	7	0.030	0.0037	0.020
6.5	0.16×10^{-7}	2.3×10^4	0.0158	8	0.034	0.0023	0.025
6.5	0.25×10^{-7}	2.3×10^4	0.0158	8	0.034	0.0036	0.030
6.8	0.28×10^{-7}	2.4×10^4	0.0172	9	0.040	0.0040	0.030
7.0	0.14×10^{-7}	2.4×10^4	0.0183	9	0.046	0.0021	0.030
7.1	0.85×10^{-7}	2.5×10^4	0.0189	9	0.049	0.0124	0.030
7.5	0.30×10^{-7}	2.6×10^4	0.0201	10	0.055	0.0044	0.045
8.1	0.56×10^{-7}	2.8×10^4	0.0220	11	0.066	0.0081	0.045

Other expressions employed here are the ones proposed by Bagnold (1956) and by Lettau and Lettau (1978). Bagnold (1956) proposed that $\phi_B = \eta\theta^{1/2}(\theta-\theta_{th})$ where η is given by $\eta \approx A(2/3\ \mu_s/C_D)^{1/2}$. A is a constant that depends on the Reynolds number and is taken here as 5.5 (Bagnold, 1956), μ_s is the friction between grains, and C_D is the drag factor for the grains. Lettau and Lettau (1978) proposed $\phi_B = \chi\theta(\theta-\theta_{th})^{1/2}$, where $\chi = C_L((S-1)gd)^{3/2}\rho/g$ and C_L is a constant to be adjusted and taken here as 12.

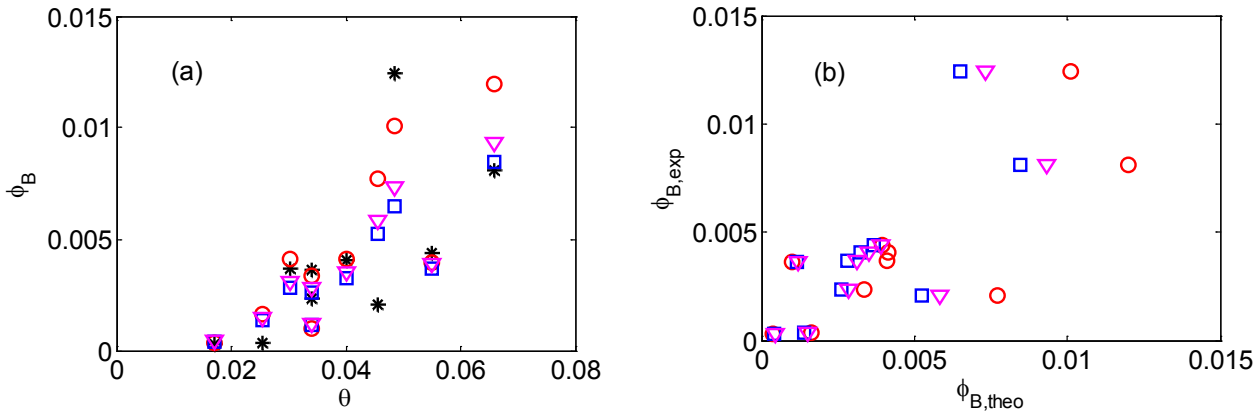

Figure 3. (a) Dimensionless bed-load transport rate ϕ_B as function of Shields number θ. (b) Measured bed-load transport rate (dimensionless) $\phi_{B,exp}$ as function of theoretical bed-load transport rate (dimensionless) $\phi_{B,theo}$.

Figure 3(a) presents the dimensionless bed-load transport rate ϕ_B as function of the Shields number θ. The asterisks, circles, squares and inverted triangles correspond to measured values of this study (computed from individual grains), and to the Meyer-Peter and Müller (1948), Bagnold (1956) and Lettau and Lettau (1978) expressions, respectively. Figure 3(b) presents the measured bed-load transport rate (dimensionless) $\phi_{B,exp}$ as function of the theoretical (semi-empirical expressions) bed-load transport rate (dimension-

less) $\phi_{B,theo}$. The circles, squares and inverted triangles correspond to comparisons with the Meyer-Peter and Müller (1948), Bagnold (1956) and Lettau and Lettau (1978) expressions, respectively. The experimentally determined bed-load transport rates are in good agreement with semi-empirical expressions proposed in the literature, corroborating the measurements for individual grains.

4 CONCLUSIONS

This paper was devoted to the trajectories of individual grains of a moving granular layer under a turbulent water flow. Experiments were performed in a closed conduit, where fully-developed turbulent water flows were imposed over a granular bed of known granulometry. The water stream was measured by Particle Image Velocimetry (Franklin et al., 2014) and the displacements of grains were filmed with a high-speed camera. The trajectories and velocities of individual grains were determined by post-processing the images and the shear stress caused by the fluid on the bed was estimated from the PIV data. The experimental results showed that individual grains have an intermittent motion, with periods of acceleration, deceleration and at rest. The typical traveled distances, displacement times and velocities were computed based on the trajectories of individual grains. The bed-load transport rate was estimated on the basis of the measured motions and correlated with water flow conditions. The experimentally determined bed-load transport rates were compared with semi-empirical expressions proposed in the literature and they were found to agree well.

NOTATION

ρ	specific mass of the fluid
ρ_s	specific mass of grains
S	ratio of specific masses
g	gravity acceleration
u_*	shear velocity
ϕ_B	dimensionless bed-load transport rate
$\phi_{B,exp}$	dimensionless bed-load transport rate, measured
$\phi_{B,theo}$	dimensionless bed-load transport rate, theoretical
τ	shear stress caused by the fluid on the granular bed
Q	water flow rate
Q_B	bed-load transport rate
Re	Reynolds number
Re_*	particle Reynolds number
θ	Shields number
θ_{th}	threshold Shields number
Δx	mean longitudinal displacement of grains
Δx^{ad}	normalized longitudinal displacement of grains
t	time
t_d	displacement time
t_d^{ad}	normalized displacement time
U_d	mean displacement velocity
U_d^{ad}	normalized displacement velocity
N_L	number of black spheres that crossed a transverse line during the total time of the movie
f	movie frequency
$\sigma_\Delta x$	standard deviation of the longitudinal displacement
σ_{Ud}	standard deviation of the longitudinal velocity
d	grain diameter
d_{50}	mean grain diameter
u	mean fluid velocity
u^+	normalized fluid velocity
$\bar{U}$	mean cross-section velocity of the fluid
y	vertical coordinate
ν	kinematic viscosity
κ	von Kármán constant
y_0	roughness length
a	constant
A	constant
B	constant
C_L	constant
C_D	drag factor for the grains

η Bagnold coefficient (Bagnold, 1956)
χ Lettau and Lettau coefficient (Lettau and Lettau, 1978)

ACKNOWLEDGEMENTS

The authors are grateful to FAPESP (grants nos. 2012/19562-6 and 2013/05479-2) to FAEPEX/UNICAMP (conv. 519.292, project 0201/14) and to CAPES for the provided financial support.

REFERENCES

Bagnold, R.A. (1941). The physics of blown sand and desert dunes. Chapman and Hall, London, UK, 265 pages.

Bagnold, R.A. (1956). The flow of cohesionless grains in fluids. Proc. Royal Soc. Lond. Vol. 249, pp. 235-297.

Bauer, B. O., Houser, C. A., Nickling, W. G. (2004). Analysis of velocity profile measurements from wind-tunnel experiments with saltation. Geomorphology, Vol. 49, pp. 81-98.

Charru, F. Mouilleron, H. and Eiff, O. (2004). Erosion and deposition of particles on a bed sheared by a viscous flow. J. Fluid Mech., Vol.519, pp. 55-80.

Clift, R., Grace, J., Weber, M. (2005). Bubbles, drops and particles. Dover Publications, Mineola, USA, 400 pages.

Franklin, E.M., Figueiredo, F.T., Rosa, E.S. (2014). The feedback effect caused by bed load on a turbulent liquid flow", J. Braz. Soc. Mech. Sci. Eng., accepted.

Gomez, B., Church, M. (1989). An assessment of bed load sediment transport formulae for gravel bed rivers. Water Resour. Res., Vol.25, pp. 1161-1186.

Lettau, K., Lettau, H. (1978). Experimental and micrometeorological field studies of dune migration. In: H. H. Lettau and K. Lettau (Eds.), Exploring the World's Driest Climate, Center for Climatic Research, Univ. Wisconsin: Madison, pp. 110-147.

Meyer-Peter, E. and Müller. (1948). Formulas for bed-load transport. Proceedings of the 2nd Meeting of International Association for Hydraulic Research, Stockholm, Sweden, pp. 39-64.

Nakato, T. (1990). Tests of selected sediment-transport formulas. J. Hydraul. Eng., Vol.116, pp. 362-379.

Rasmunsen, K. R., Iversen, J. D., Rautahemio, P. (1996). Saltation and wind flow interaction in a variable slope wind tunnel. Geomorphology, Vol.17, pp. 19-28.

Raudkivi, A.J. (1976). Loose Boundary Hydraulics. Pergamon Press, Oxford, UK, 397 pages.

Recking, A., Frey, P, Paquier, A., Belleudy, P., Champagne, J.Y. (2008). Feedback between bed load transport and flow resistance in gravel and cobble bed rivers. Water Resour. Res., Vol.44, W05412.

Wong, M., Parker, G. (2006). Reanalysis and correction of bed-load relation of Meyer-Peter and Müller using their own database. J. Hydraul. Eng., Vol.132, pp. 1159-1168.

Yang, P., Dong, Z., Qian, G., Luo, W., Wang, H. (2007). Height profile of the mean velocity of an aeolian salting cloud: wind tunnel measurements by Particle Image Velocimetry. Geomorphology, Vol.89, pp. 320-334.